

## GAMMA-RAY EMISSION PROPERTIES FROM MATURE PULSARS IN THE GALAXY AND IN THE GOULD BELT

K. S. CHENG,<sup>1</sup> L. ZHANG,<sup>2,3</sup> P. LEUNG,<sup>1</sup> AND Z. J. JIANG<sup>3</sup>

Received 2003 August 16; accepted 2004 February 23

### ABSTRACT

We study the  $\gamma$ -ray emission properties of pulsars by using a new self-consistent outer gap model. The outer gap can exist in pulsars older than 1 million yr if the effect of magnetic inclination angle, as well as the average properties of the outer gap, are considered. The mature  $\gamma$ -ray pulsars, whose ages are between 0.3 and 3 million yr, are able to move up to high Galactic latitude. Moreover, their  $\gamma$ -ray luminosities are weaker, and their spectra are significantly softer than those of younger  $\gamma$ -ray pulsars in the Galactic plane. We use a Monte Carlo method to simulate the statistical properties of  $\gamma$ -ray pulsars in the Galaxy as well as in the Gould Belt. We find that  $\gamma$ -ray pulsars located at  $|b| < 5^\circ$  and  $|b| > 5^\circ$  have very different properties. High Galactic latitude  $\gamma$ -ray pulsars are dominated by mature pulsars with longer periods, weaker fluxes, and softer spectra. If the pulsar birth rates in the Galaxy and the Gould Belt are  $\sim 10^{-2}$  and  $\sim 2 \times 10^{-5}$  yr<sup>-1</sup>, respectively, there are 42 and 35 radio-quiet  $\gamma$ -ray pulsars for  $|b| < 5^\circ$  and  $|b| > 5^\circ$ , respectively. The number of radio-quiet  $\gamma$ -ray pulsars from the Gould Belt are 2 and 13 for  $|b| < 5^\circ$  and  $|b| > 5^\circ$ , respectively. We suggest that a good fraction of unidentified EGRET  $\gamma$ -ray sources may be these radio-quiet  $\gamma$ -ray pulsars. Furthermore,  $\gamma$ -ray pulsars located at  $|b| > 5^\circ$  satisfy  $L_\gamma \propto L_{\text{sd}}^\beta$ , whereas  $L_\gamma \propto L_{\text{sd}}^\delta$  for  $\gamma$ -ray pulsars in the Galactic plane, where  $\beta \sim 0.6$  and  $\delta \sim 0.3$ , respectively.

*Subject headings:* gamma rays: theory — pulsars: general — stars: neutron — stars: statistics

### 1. INTRODUCTION

There are 170 unidentified  $\gamma$ -ray sources in the third EGRET catalog (Hartman et al. 1999):  $\sim 50$  sources close to the Galactic plane with  $|b| < 5^\circ$ , and  $\sim 70$  sources in the medium latitudes with  $|b|$  between  $5^\circ$  and  $30^\circ$ . For those unidentified  $\gamma$ -ray sources in the Galactic plane, many are associated with Wolf-Rayet and Of stars, SNRs, and OB stars (Montmerle 1979; Kaaret & Cottam 1996; Yadigaroglu & Romani 1997; Romero et al. 1999). Most of these objects are considered pulsar tracers; therefore, it is natural to suggest that these low-latitude sources may be Geminga-like pulsars, which are radio-quiet pulsars (Yadigaroglu & Romani 1995; Cheng & Zhang 1998; Zhang et al. 2000). Since  $\gamma$ -ray pulsars are known to be steady  $\gamma$ -ray emitters, it has been suggested that the variability should be a good indicator for distinguishing the real pulsar candidates from the unidentified EGRET sources (Romero et al. 1994; McLaughlin et al. 1996; Zhang et al. 2000; Torres et al. 2001; Nolan et al. 2003). Gehrels et al. (2000) define a class of sources as steady if the most significant detection of a source in 3EG catalog is for a timescale of years, and if that particular flux is within  $3\sigma$  of the flux calculated for the full data set. From this classification, 48 unidentified sources at  $|b| < 5^\circ$  and 72 unidentified sources at  $|b| > 5^\circ$  are steady sources, respectively. On the other hand, Grenier (2000) suggests another definition, persistent sources, which are detected sources with a significance  $(TS)^{1/2} > 4$  for every observation at  $|b| > 2.5^\circ$ . If we assume that the sources with a significance  $(TS)^{1/2} > 5$  at  $|b| \leq 2.5^\circ$  are persistent sources, there are 40 (45) persistent unidentified EGRET sources at  $|b| < 5^\circ$  ( $|b| > 5^\circ$ ).

However, the spectral properties of medium-latitude sources are significantly softer, fainter, and have a steeper  $\log N - \log S$  function than those at low latitudes (Gehrels et al. 2000). It has been suggested that they are associated with recent supernovae in the nearby Gould Belt (Grenier 1997, 2000; Gehrels et al. 2000). Their natures remain a mystery. Harding & Zhang (2001) used the polar cap models (Daugherty & Harding 1996; Harding & Muslimov 1998) to investigate whether  $\gamma$ -ray pulsars viewed at a large angle to the neutron star magnetic pole could contribute to unidentified EGRET sources in the medium latitudes associated with the Gould Belt. They suggest that the off-beam  $\gamma$ -rays come from high-altitude curvature emission of primary particles that can radiate over a large solid angle and have a much softer spectrum than that of the main beams, and at least some of the radio-quiet Gould Belt sources detected by EGRET could be such off-beam  $\gamma$ -ray pulsars.

Recently, the brightest of unidentified EGRET sources in medium latitude, 3EG J1835+5918, is strongly considered the second Geminga-like pulsar (radio-quiet pulsar) by multi-wavelength observations, including *Chandra*, the *Hubble Space Telescope*, and Jodrell Bank (Mirabel et al. 2000; Mirabal & Halpern 2001; Halpern et al. 2002). The X-ray spectrum can be described by two components: a soft thermal X-ray spectrum with a characteristic temperature ( $T_{\text{inf}} \approx 3 \times 10^5$  K), and a power-law hard tail with a photon index  $\gamma \approx 2$ , which closely resembles the X-ray spectrum of Geminga. The repeated radio observations at Jodrell Bank did not show any periodicity. The X-ray data suggest that the distance is between 250 and 800 pc, which is consistent with the distance to the Gould Belt.

In this paper, we use the revised outer gap models (Zhang et al. 2004) to investigate the emission properties of  $\gamma$ -ray pulsars in the Galaxy as well as in the Gould Belt. This revised outer gap model is based on the original outer gap models (Cheng et al. 1986a, hereafter CHRI, 1986b; Zhang & Cheng 1997) but takes into account the effect of the inclination angle ( $\alpha$ ), which is the angle between the magnetic axis and the

<sup>1</sup> Department of Physics, the University of Hong Kong, Hong Kong, People's Republic of China.

<sup>2</sup> National Astronomical Observatories/Yunnan Observatory, Chinese Academy of Sciences, P.O. Box 110, Kunming, People's Republic of China.

<sup>3</sup> Department of Physics, Yunnan University, Kunming, People's Republic of China.

rotation axis, in determining the size of the outer gap, which is defined as the ratio between the dimension of the gap perpendicular to the magnetic field and the light cylinder radius. The revised model also takes into account the fact that the typical radiation region of the outer gap is not necessary at half of the light cylinder; instead, it should be better represented by an appropriate average over the entire outer gap. This effect is particularly important for old pulsars. If the outer gap is only represented at half of the light cylinder, then the outer gap is assumed to be turned off when the gap size at this region is larger than unity. This new model has taken the entire active region of the outer gap into account. As long as the gap size is less than unity in some parts of the magnetosphere, the outer gap still exists. This effect allows some pulsars with appropriate combinations of  $\alpha$ ,  $P$ , and  $B$  to maintain their outer gaps until they are a few million years old. These pulsars are able to move up to high Galactic latitude, and their ages make them weak  $\gamma$ -ray sources. Furthermore, we show that these pulsars emit softer spectra and that the relation between  $\gamma$ -ray luminosity and spin-down power differs from that of younger pulsars located in the Galactic plane. We organize the paper as follows. In § 2, we review the new outer gap models. In § 3, we study the  $\gamma$ -ray emission properties of pulsars by using the new self-consistent outer gap model. In § 4, we describe a Monte Carlo simulation method to determine the statistical distributions of radio-quiet and radio-loud  $\gamma$ -ray pulsars. In § 5, we summarize the simulation results and discuss their implications. Finally, a brief conclusion is given in § 6.

## 2. OUTER GAP MODELS

Zhang & Cheng (1997) have proposed a self-consistent mechanism to describe the high-energy radiation from rotation-powered pulsars. In this model, the radiation mechanism of relativistic charged particles from a thick outer magnetospheric accelerator (outer gap) is synchrocurvature radiation (Cheng & Zhang 1996), and the characteristic energy of high-energy photon emitted from the outer gap is determined by the pulsar global parameters, i.e., the rotation period  $P$  and the dipolar magnetic field  $B$ , as well as the fractional size of the outer gap ( $f$ ), which is the ratio between the mean vertical separation of the outer gap boundaries in the plane of the rotation axis and the magnetic axis to the light cylinder radius, and is given by

$$E_\gamma(f) \approx 5.0 \times 10^7 f^{3/2} B_{12}^{3/4} P^{-7/4} \left(\frac{r}{R_L}\right)^{-13/8} \text{ eV}, \quad (1)$$

where  $B_{12}$  is the dipolar magnetic field in units of  $10^{12}$  G,  $R_L$  is the light cylinder radius, and  $r$  is the distance to the neutron star. The  $\gamma$ -ray spectrum becomes exponentially decayed beyond  $E_\gamma(f)$ . The fractional size of the outer gap determines the total  $\gamma$ -ray luminosity from the outer gap (Zhang & Cheng 1997) and is given by

$$L_\gamma = f^3 L_{\text{sd}}, \quad (2)$$

where  $L_{\text{sd}} = 3.8 \times 10^{31} B_{12}^2 P^{-4}$  ergs s $^{-1}$  is the spin-down power of pulsar. CHRI have shown that the inner boundary of the static outer gap begins at the null charge surface ( $\mathbf{\Omega} \cdot \mathbf{B} = 0$ ). Recently, Hirovani & Shibata (2001) have shown that if there is injected current from the inner boundary, the position of the inner boundary can shift either toward the star or even closer to the light cylinder depending on the sign and the magnitude of the injected current. However, it is not clear what causes this

injected current. In this paper we assume that the outer gap begins at the null charge surface. The radial distance from the null surface to the star is  $r_{\text{in}}$ , which is a function of the magnetic inclination angle  $\alpha$  and is given by  $r_{\text{in}}/R_L = \sin^2(\theta_{\text{in}} - \alpha)/[\sin \theta_c \sin^2(\theta_c - \alpha)]$ , where  $\theta_{\text{in}}$  is the polar angle of  $r_{\text{in}}$  determined by  $\tan \theta_{\text{in}} = \frac{1}{2}[3 \tan \alpha + (9 \tan^2 \alpha + 8)^{1/2}]$  and  $\theta_c$  is the polar angle to the position where the first open field line intercepts the light cylinder determined by  $\tan \theta_c = -(3/4 \tan \alpha)[1 + (1 + 8 \tan^2 \alpha/9)^{1/2}]$ . The fractional size of the outer gap is limited by the pair production between the soft thermal X-rays with characteristic energy  $E_X$  from the stellar surface and the high-energy photons with energy  $E_\gamma(f_0)$  emitted from the outer gap. The energy of the soft X-ray photons is determined by the backflow of the primary electrons/positrons. Each of these backflow particles can still maintain about  $10.6P^{1/3}$  ergs and deposit on the stellar surface. This energy will be emitted as soft thermal X-rays from the stellar surface (Halpern & Ruderman 1993), whose characteristic energy is given by  $E_X(f_0) \approx 1.2 \times 10^2 f_0^{1/4} B_{12}^{1/4} P^{-5/12}$  eV. Although the thermal X-ray photon density is low, every pair resulting from X-ray and high-energy photon interactions can emit  $\sim 10^5$  high-energy photons when they are accelerated in the gap. Such a large multiplicity can produce a sufficient number of  $e^\pm$  pairs to sustain the outer gap. Assuming  $r = R_L/2$  and head-on collision, they obtained the fractional size of the outer gap as

$$f_0(B, P) \approx 5.5 P^{26/21} B_{12}^{-4/7} \quad (3)$$

from the condition of photon-photon pair production,  $E_X E_\gamma [1 - \cos(\theta_{X\gamma})] = 2(m_e c^2)^2$ .

However, this model did not take into account the fact that when the magnetic inclination angle ( $\alpha$ ) becomes large, the characteristic energy of high-energy photons from the gap, which depends on  $\alpha$ , also increases. In fact, both  $E_X$  and  $\theta_{X\gamma}$  also depend on  $\alpha$ . Most important, Zhang & Cheng (1997) have assumed a typical distance ( $r = R_L/2$ ) to represent the outer gap. In other words, most radiation and pair production activities are assumed to take place at this characteristic region. They assume that when  $f_0(r = R_L/2, B, P) > 1$ , the outer gap does not exist. However, even the mid-distance to the outer gap depends on the inclination angle, because the outer gap begins at the null charge surface, which depends on  $\alpha$ . Realistically, as long as  $e^\pm$  pairs can be produced beyond the null surface, the outer gap should be still active, namely, accelerating charged particles. Of course, for regions with  $f(r) > 1$ , the gap potential should drop off rapidly and hence becomes unimportant. Therefore, the active region of the outer gap should begin at null surface and stop at a distance  $r_b$  where  $f(r_b) = 1$  (Zhang et al. 2004). In explaining the detailed  $\gamma$ -ray spectrum of a given pulsar, it is important to know from which parts of the pulsar magnetosphere the radiation comes (Cheng et al. 2000). However, in order to study the statistical properties of pulsars, a representative region is a very useful approximation. They assume that the representative region of the outer gap is the average distance to the gap; they obtain the mean fractional size of the gap  $f(P, B, \alpha)$ , which can be approximately expressed as

$$f(\alpha, B, P) \approx f_0(B, P) \eta(\alpha, B, P), \quad (4)$$

where  $\eta(\alpha, B, P)$  is a monotonic function of  $\alpha$ ,  $B$ , and  $P$ . It roughly decreases by a factor of 3 from young pulsars with large inclination angles to old pulsars with small inclination angles. The integral expression of  $f(\alpha, B, P)$  is given by

equation (38), and the variation of  $\eta$  for different pulsars is given in Figure 3 of Zhang et al. (2004), respectively. Although the variation of  $\eta$  is only a factor of 3, the implications are very important. First, the cutoff period of  $\gamma$ -ray pulsars is about a factor of  $3^{21/26} = 2.4$  longer for fixed  $\alpha$  and  $B$ , compared to the old model. Second, the cutoff age of  $\gamma$ -ray pulsars is about a factor of 5.8 longer as well. This means that there are many more  $\gamma$ -ray pulsars in high Galactic latitude than previously expected. These older  $\gamma$ -ray pulsars can move up to high Galactic latitude and may contribute to the unidentified EGRET sources.

### 3. GAMMA-RAY EMISSION PROPERTIES OF MATURE PULSARS

Inside the thick outer gap (Zhang & Cheng 1997),  $\gamma$ -rays are produced by curvature radiation from the primary  $e^\pm$  pairs along the curved magnetic field lines. However, Cheng & Zhang (1996) studied the radiation from the charged particles in the curved magnetic field and noted that the radiation should be described more accurately by a general radiation mechanism called synchrocurvature radiation mechanism, in which the radiation is being emitted by the charged particles moving in a spiral trajectory along the curved magnetic field lines. This mechanism differs from synchrotron and curvature mechanisms in general but reduces to either synchrotron radiation when the radius of curvature of the local magnetic field lines is infinite, or to curvature radiation when the pitch angle is zero. In fact, when the synchrotron gyroradius  $r_B = \gamma mc^2 \sin \theta_p / eB(r)$  and the curvature radius of the field  $s \approx (rR_L)^{1/2}$  are comparable, the synchrocurvature mechanism really provides a significant improvement, where  $\gamma$  is the Lorentz factor of the accelerated particles and  $\theta_p$  is the pitch angle of the charged particles in the curved magnetic field. Zhang & Cheng (1997) used this mechanism to describe the production of nonthermal photons from the primary  $e^\pm$  pairs along the curved magnetic field lines in the outer gap. The primary  $e^\pm$  pairs have an approximate power-law distribution inside the outer gap, because the energy and density of the primary  $e^\pm$  pairs depend on local values of the magnetic field, the electric field, and the radius of curvature. In steady state, the energy distribution of the accelerated particles in the outer gap is  $(dN/dE_e) \propto E_e^{-16/3}$ , where  $E_e$  is the energy of the accelerated particles. Using the general formula of the synchrocurvature radiation power spectrum given by Cheng & Zhang (1996) and  $(dN/dE_e)dE_e = (dN/dx)dx$ , where  $x = s/rR_L$ , the differential flux at the Earth is (Zhang & Cheng 1997)

$$F(E_\gamma) \approx \frac{1}{\Delta\Omega d^2} \frac{\dot{N}_0}{E_\gamma} \int_{x_{\min}}^{x_{\max}} \left\{ x^{3/2} \frac{R_L}{R_c} \left[ \left( 1 + \frac{1}{R_c^2 Q_2^2} \right) F(y) - \left( 1 - \frac{1}{R_c^2 Q_2^2} \right) y K_{2/3}(y) \right] \right\} dx, \quad (5)$$

where  $\Delta\Omega$  is the solid angle of  $\gamma$ -ray beaming,  $d$  is the distance to the pulsar,  $\dot{N}_0 = \sqrt{3}e^2\gamma_0 N_0 / hR_L$ ,  $N_0 \approx 1.4 \times 10^{30} f(B_{12}/P) R_6^3$ ,  $\gamma_0 \approx 2 \times 10^7 f^{1/2} (B_{12}/P)^{1/4}$ ,  $R_c = xR_L / \{ [1 + r_B/(xR_L)] \cos^2 \theta_p + (R_L/r_B)x \sin^2 \theta_p \}$ ,  $Q_2 = (1/xR_L) \{ (r_B/xR_L) + 1 - 3(R_L/r_B)x \cos^4 \theta_p + 3(R_L/r_B)x \cos^2 \theta_p + (R_L/r_B)^2 x^2 \sin^4 \theta_p \}^{1/2}$ , and  $\sin \theta_p \approx 0.79 f^{1/2} B_{12}^{-3/4} P^{1/4} x^{17/4}$ ;  $F(y) = \int_y^\infty K_{5/3}(z) dz$ , where  $K_{5/3}$  is the modified Bessel function of order 5/3,  $y = E_\gamma/E_c$ , and  $E_c = (3/2)(\hbar c \gamma^3/x)(xQ_2)$  is the characteristic energy of the synchrocurvature photons. The quantities  $x_{\min}$  and  $x_{\max}$  are the minimum and maximum values of  $x$ ;  $x_{\min}$

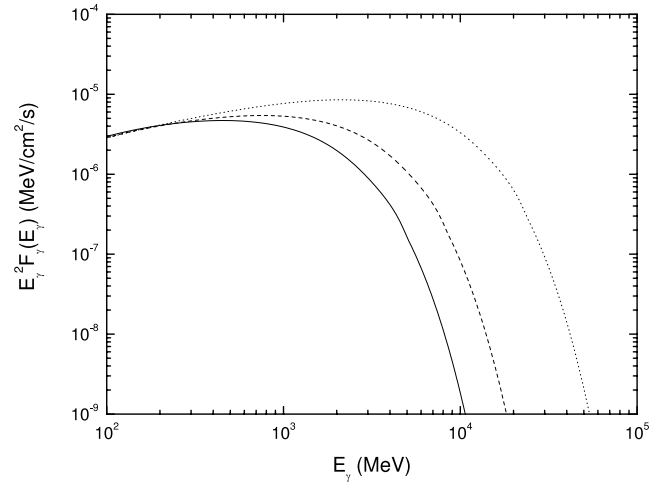


FIG. 1.—Distribution of energy flux vs. energy of the photon. In this figure,  $B_{12}$  is 3,  $P$  is 0.4 s, and  $\alpha$  is  $20^\circ$  (solid line),  $40^\circ$  (dashed line), and  $60^\circ$  (dotted line).

can be estimated as  $x_{\min} = (r_{\text{in}}/R_L)^{1/2}$ . The maximum value of  $x$  can be estimated by  $x_{\max} \approx \theta_p/\theta_f (r_f/R_L)^{1/2}$  (Arons & Scharlemann 1979), where  $\theta_p$  is the angular width of the polar cap,  $\theta_f$  is the angular width between the magnetic axis to the upper boundary field lines of the outer gap, and  $r_f$  is the radial distance to the upper boundary field lines intercepting the light cylinder. Zhang & Cheng (1997) have discussed the possible value of  $x_{\max}$ . In general, the  $\gamma$ -ray beaming solid angle should be different for various  $\gamma$ -ray pulsars, which is a function of the magnetic inclination angle as well as the size of the outer gap (Zhang et al. 2004). Some approximate forms of beaming solid angles have been given (Yadigaroglu & Romani 1995; Zhang et al. 2000). The accuracy of these approximation forms are not known. For simplicity, in this paper we treat these two parameters,  $\Delta\Omega$  and  $x_{\max}$ , as constants. By fitting the  $\gamma$ -ray spectrum of known  $\gamma$ -ray pulsars, these two parameters are  $\Delta\Omega \sim 1$  sr and  $x_{\max} \sim 2$ , respectively (Cheng & Zhang 1998).

In order to compare our results with the EGRET data, the integral flux is necessary and is given by

$$F(\geq 100 \text{ MeV}) = \int_{100 \text{ MeV}}^{E_{\max}} F(E_\gamma) dE_\gamma, \quad (6)$$

where  $E_{\max}$  is the maximum energy of  $\gamma$ -rays and is chosen to be 100 GeV.

In Figures 1, 2, and 3, the model  $\gamma$ -ray spectra are calculated for various periods, magnetic fields, and inclination angles, respectively. We can see that the spectra become softer when the period decreases, the magnetic field increases, or the inclination angle decreases in the energy range of EGRET (100 MeV–10 GeV). Alternatively speaking, the spectral break becomes larger when the period increases, the magnetic field decreases, or the inclination angle increases. We can understand these trends by examining the behavior of the energy break at equation (1). Typically, most of the power radiated from the primary electrons/positrons comes from regions with characteristic distance of the order of  $\sim R_L$ . Substituting equations (3) and (4) into equation (1), we obtain the spectral break  $\propto \eta^{3/2} P^{3/28} B_{12}^{-3/28}$ , which explains the relations between spectral variations in Figures 1–3. However, in §§ 4–5, we find that the key differences between  $\gamma$ -ray

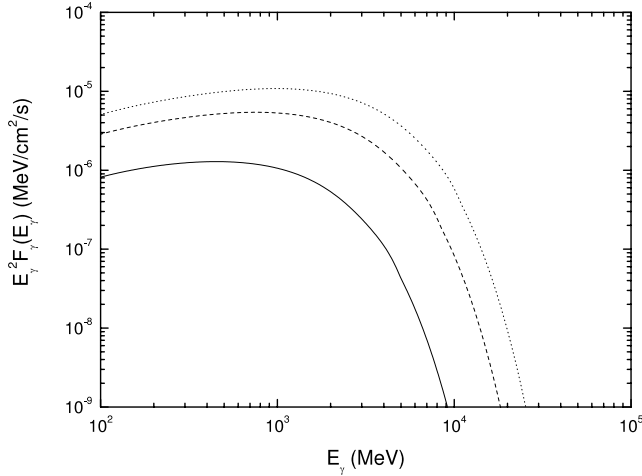


FIG. 2.—Distribution of energy flux vs. energy of the photon. In this figure,  $P$  is 0.4 s,  $\alpha$  is  $40^\circ$ , and  $B_{12}$  is 1 (solid line), 3 (dashed line), and 5 (dotted line).

pulsars in the Galactic plane and those in high Galactic latitude are (1) Galactic plane  $\gamma$ -ray pulsars are younger, shorter in period, and have larger inclination angles; and (2) they satisfy a different relation between  $L_\gamma$  and  $L_{sd}$ . In fact, most high-latitude  $\gamma$ -ray pulsars satisfy  $L_\gamma \propto L_{sd}$ , which means  $f \sim 1$  (cf. Fig. 6f and Fig. 7, bottom panel). In this case, the spectral break is  $\propto \eta^{21/16} P^{-1/8}$ . Since Galactic  $\gamma$ -ray pulsars have larger inclination angles and shorter periods compared with the high Galactic latitude  $\gamma$ -ray pulsars, the spectra of  $\gamma$ -ray pulsars in high Galactic latitude have a softer spectrum than those in the Galactic plane. In Figure 4, we compare the typical spectra between the high and low Galactic latitude  $\gamma$ -ray pulsars.

#### 4. MONTE CARLO SIMULATION OF GAMMA-RAY PULSARS IN THE GALAXY AND IN THE GOULD BELT

In order to consider the  $\gamma$ -ray luminosity and spatial evolution of pulsars in the Galaxy and in the Gould Belt, the initial values of parameters of pulsar at birth, which include the initial position, velocity, period, and magnetic field strength,

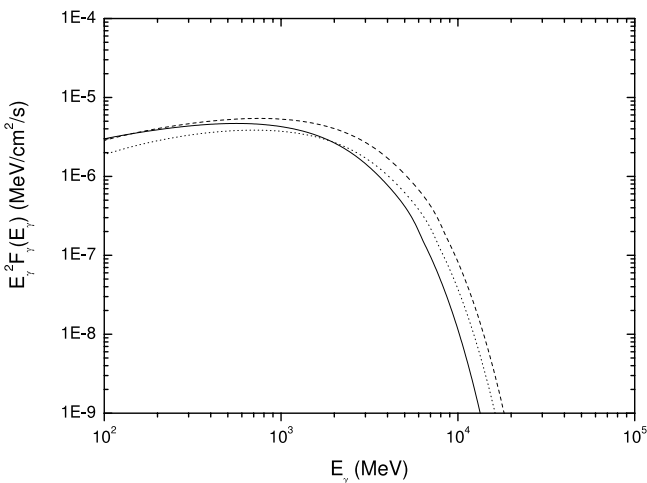


FIG. 3.—Distribution of energy flux vs. energy of the photon. In this figure,  $B_{12}$  is 3,  $\alpha$  is  $40^\circ$ , and  $P$  is 0.2 s (solid line), 0.4 s (dashed line), and 0.6 s (dotted line).

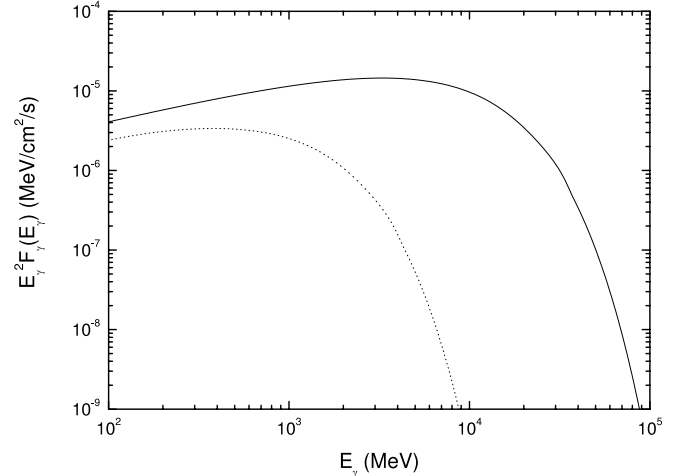


FIG. 4.—Distribution of energy flux vs. energy of the photon. The solid line is the typical photon spectrum of a Galactic  $\gamma$ -ray pulsar with  $B_{12} = 5$ ,  $P = 0.1$  s, and  $\alpha = 70^\circ$ , and the dashed line is the typical photon spectrum of a  $\gamma$ -ray pulsar in high Galactic latitude with  $B_{12} = 2$ ,  $P = 0.3$  s, and  $\alpha = 20^\circ$ , respectively.

are needed. The Monte Carlo method and the evolution of pulsar parameters are described in our previous works (Cheng & Zhang 1998; Zhang & Cheng 1999; Zhang et al. 2000, 2004; Fan et al. 2001). Here, we briefly describe basic assumptions for generating the  $\gamma$ -ray pulsars (radio-quiet and radio-loud) in the Galaxy as well as in the Gould Belt:

1. The pulsars are born at a rate ( $\dot{N}_{NS} \sim 1$  per century) in the Galaxy. The age of the Gould Belt is estimated at  $\sim 30$  Myr old, and the pulsars are born at a rate of  $\sim 20$  Myr $^{-1}$  (Grenier 2000).

2. The Gould Belt has an ellipsoidal ring with semimajor and minor axes equal to 500 and 340 pc, respectively. The Sun is displaced from the center of Gould Belt about 200 pc toward  $l = 130^\circ$  (Guilout et al. 1998). On the other hand, there are other possible interpretations for the geometry of the Gould Belt. For example, Olano (1982) and Moreno et al. (1999) have given a smaller size for the Gould Belt. However, we will show that most  $\gamma$ -ray pulsars originating from the Gould Belt are mature pulsars nearly 1 million yr old. They already move very far away from the Gould Belt. The most important point is that our solar system is enclosed in the Gould Belt; the exact dimensions of the Gould Belt are not crucial to our problem.

3. The initial position of each pulsar in the Galaxy is estimated from the distributions  $\rho_z(z) = (1/z_{\text{exp}}) \exp(-|z|/z_{\text{exp}})$  and  $\rho_R(R) = (a_R/R_{\text{exp}}^2) \exp(-R/R_{\text{exp}})$ , where  $z$  is the distance from the Galactic plane,  $R$  is the distance from the Galactic center,  $z_{\text{exp}} = 75$  pc,  $a_R = [1 - e^{-R_{\text{max}}/R_{\text{exp}}}(1 + R_{\text{max}}/R_{\text{exp}})]^{-1}$ ,  $R_{\text{exp}} = 4.5$  kpc, and  $R_{\text{max}} = 20$  kpc (Paczynski 1990; Sturmer & Dermer 1996). However, the initial position of each pulsar is assumed to be born uniformly inside the Gould Belt.

4. The initial magnetic fields are distributed as a Gaussian in  $\log B$  with a mean value of 12.5 and a dispersion of 0.3. Since the majority of  $\gamma$ -ray pulsars are younger than 3 million yr old and the field does not decay in 10 Myr (Bhattacharya et al. 1992), we ignored any field decay for these rotation-powered pulsars.

5. The initial period is  $P_0 = 10$  ms, and the period at time  $t$  is given by  $P(t) = (P_0 + 1.95 \times 10^{-39} B^2 t)^{1/2}$ . We note that the

initial period is not crucial for our problem, because the typical age of  $\gamma$ -ray pulsars is of the order of 1 million yr old.

6. The initial velocity of each pulsar is the vector sum of the circular rotation velocity at the birth location and random velocity from the supernova explosion (Paczynski 1990). The circular velocity is determined by Galactic gravitational potential, and the random velocity is distributed as a Maxwellian distribution with a dispersion of three-dimensional velocity  $= \sqrt{3} \times 100 \text{ km s}^{-1}$  (Lorimer et al. 1997). Furthermore, the pulsar position at time  $t$  is determined following its motion in the Galactic gravitational potential. Using the equations given by Paczynski (1990) for a given initial velocity, the orbit integrations are performed by using the fourth-order Runge-Kutta method with variable time steps (Press et al. 1992) on the variables  $R$ ,  $V_R$ ,  $z$ ,  $V_z$ , and  $\phi$ . Then the sky position and the distance of the simulated pulsar can be calculated.

7. The inclination angle ( $\alpha$ ) of each pulsar is chosen randomly from a uniform distribution (Biggs 1990).

8. The following radio selection effects are used. The pulsar must satisfy the condition that its radio flux is greater than the radio survey flux threshold and that its broadened pulse width is less than the rotation period (e.g., Sturmer & Dermer 1996). We calculate the 400 MHz radio luminosity,  $L_{400}$ , of each model pulsar using the following distribution given by (Narayan & Ostriker 1990),  $\rho_{L_{400}}(P, \dot{P}) = 0.5\lambda^2 e^{-\lambda}$ , where  $\lambda = 3.6[\log(L_{400}/\langle L_{400} \rangle) + 1.8]$ ,  $\log \langle L_{400} \rangle = 6.64 + (1/3)\log(\dot{P}/P^3)$ , and  $L_{400}$  is in units of mJy kpc<sup>2</sup>. The minimum detectable average flux density,  $S_{\min}$ , of a pulsar's radio survey is estimated using the method of Sturmer & Dermer (1996) (see also Cheng & Zhang 1998). The pulsar that satisfies  $L_{400}/d^2 \geq S_{\min}$  is considered a radio-detectable pulsar, where  $L_{400}$  is the radio luminosity at 400 MHz and  $d$  is the distance to the pulsar. The radio beaming fraction can be expressed as  $f_r(\omega) = (1 - \cos \omega) + (\pi/2 - \omega) \sin \omega$  (Emmering & Chevalier 1989), where  $\omega = 6^\circ 2 \times P^{-1/2}$  (e.g., Biggs 1990) is the half-angle of the radio emission cone. Then, following Emmering & Chevalier (1989), a sample pulsar with a given period  $P$  is chosen in one of the  $f_r(P)^{-1}$  cases using the Monte Carlo method. There is growing evidence that a very strong surface magnetic field exists on the surface of neutron stars. For example, absorption/emission-line features have been observed in isolated pulsars/neutron stars, e.g., 1E 1207.4–5209 (Sanwal et al. 2002), PSR 1821–24 (Becker et al. 2003), and RBS 1223 (Haberl et al. 2003). These line features imply that the surface magnetic fields are 1–2 orders of magnitude higher than those of the dipolar field. In fact, Cheng & Zhang (1999) have analyzed the X-ray emission from the polar cap regions of the rotation-powered pulsars and concluded that there exists a characteristic surface field with strength  $\sim 10^{13}$  G. Such strong surface magnetic fields can easily affect the beaming direction of the radio wave. Therefore, we assume that the beaming direction of  $\gamma$ -rays is independent of the beaming direction of the radio. In general, it is possible that there is only one beaming, either the radio or the  $\gamma$ -ray beam, pointing toward us. In fact, this is one of the key differences between outer gap and polar gap models. The solid angle of  $\gamma$ -rays is taken to be 1 sr.

9. The  $\gamma$ -ray threshold varies over the sky. Yadigaroglu & Romani (1995) used a flux threshold of  $3 \times 10^{-10} \text{ ergs cm}^{-2} \text{ s}^{-1}$ , which is comparable to the faintest  $5 \sigma$  sources in the first EGRET catalog (Fichtel et al. 1994). However, in the third EGRET catalog, the faintest source in the catalog with a significance  $(TS)^{1/2} \geq 4$  has a photon flux of  $(6.2 \pm 1.7) \times 10^{-8} \text{ cm}^{-2} \text{ s}^{-1}$  (Hartman et al. 1999). Gonthier et al. (2002) have argued that this threshold could be reduced for  $|b| > 10^\circ$ .

TABLE 1  
VARIOUS COMPONENTS OF SIMULATED GAMMA-RAY PULSARS

Parameter	Gould Belt		Galaxy	
Birth rate.....	1 50,000 yr <sup>-1</sup>		1 100 yr <sup>-1</sup>	
Galactic latitude $ b $ .....	$<5^\circ$	$>5^\circ$	$<5^\circ$	$>5^\circ$
Radio-loud.....	1	4	12	4
Radio-quiet.....	2	13	40	22

In our analysis, we include the criterion of the likelihood  $(TS)^{1/2} \geq 5$  ( $\sim 5 \sigma$ ), which corresponds to the energy threshold of  $S_\gamma^{\text{th}}(E_\gamma > 100 \text{ MeV}) \geq 1.2 \times 10^{-10} \text{ ergs cm}^{-2} \text{ s}^{-1}$  for  $|b| < 10^\circ$ , but decreases the threshold to  $S_\gamma^{\text{th}}(E_\gamma > 100 \text{ MeV}) \geq 7.0 \times 10^{-11} \text{ ergs cm}^{-2} \text{ s}^{-1}$  for  $|b| > 10^\circ$  (Gonthier et al. 2002).

## 5. SIMULATION RESULTS AND DISCUSSION

Following the procedure described in § 4, we perform a Monte Carlo simulation of Galactic pulsars born during the past  $3 \times 10^7$  yr. We use the code of Cheng & Zhang (1998) (see also Zhang et al. 2000) in our simulation, in which the Parkes Multibeam survey is not included. We summarize the various components of simulated  $\gamma$ -ray pulsars in Table 1. Our results suggest that more unidentified EGRET  $\gamma$ -ray sources should be identified as radio pulsars. In particular, the Parkes multibeam pulsar survey is expected to discover more radio pulsars (Manchester et al. 2001). Torres et al. (2001) have found five new possible radio pulsar–unidentified source associations. Most recently, Kramer et al. (2003) have used newly released survey results to correlate the unidentified EGRET  $\gamma$ -ray sources and have found more than 35 coincidences and approximately 20 probable associations. It is important to note that the number in each box of Table 1 is sensitive to the input parameters, e.g., detection threshold, birth rate, initial distributions of pulsars, etc., for a given theoretical model. However, their ratios are less sensitive to most input parameters except for their relative birth rate. It is interesting to note that the  $\gamma$ -ray pulsars in the Gould Belt contribute a significant fraction of total  $\gamma$ -ray pulsars for  $|b| > 5^\circ$  and become unimportant for  $|b| < 5^\circ$ . This is simply because the solar system is enclosed by the Gould Belt.

In Figures 5a–5e, we compare our simulated distributions of period, period derivative, magnetic field, distance, and energy flux with the observed data of eight known radio-loud  $\gamma$ -ray pulsars (i.e., Crab, Vela, Geminga, PSR 0656+14, PSR 1046–58, PSR 1055–52, PSR 1509–58, PSR 1706–44, and PSR 1951+32) using the K-S test. Although PSR 0656+14 and PSR 1509–58 are confirmed in the  $\gamma$ -ray band, there are insufficient  $\gamma$ -ray photons to provide information on the pulsed fraction, so we did not include these pulsars in the cumulative plot of energy flux. The maximum deviations of period, period derivative, magnetic field, distance, and  $\gamma$ -ray energy flux distributions from the observed distributions are 0.36, 0.32, 0.25, 0.33, and 0.21, respectively. It can be seen that four of five accumulative distributions cannot be rejected at a better than 80% confidence level, and period cumulative distribution cannot be rejected at a better than 90% confidence level. Therefore, we conclude that the model results do not conflict with the observed data of  $\gamma$ -ray pulsars.

In Figures 6a–6f, we plot the normalized distributions of period, magnetic field, age, distance, inclination angle, and the fractional size of the outer gap. The solid and dashed lines are  $\gamma$ -ray pulsars located at  $|b| < 5^\circ$  and  $|b| > 5^\circ$ , respectively.

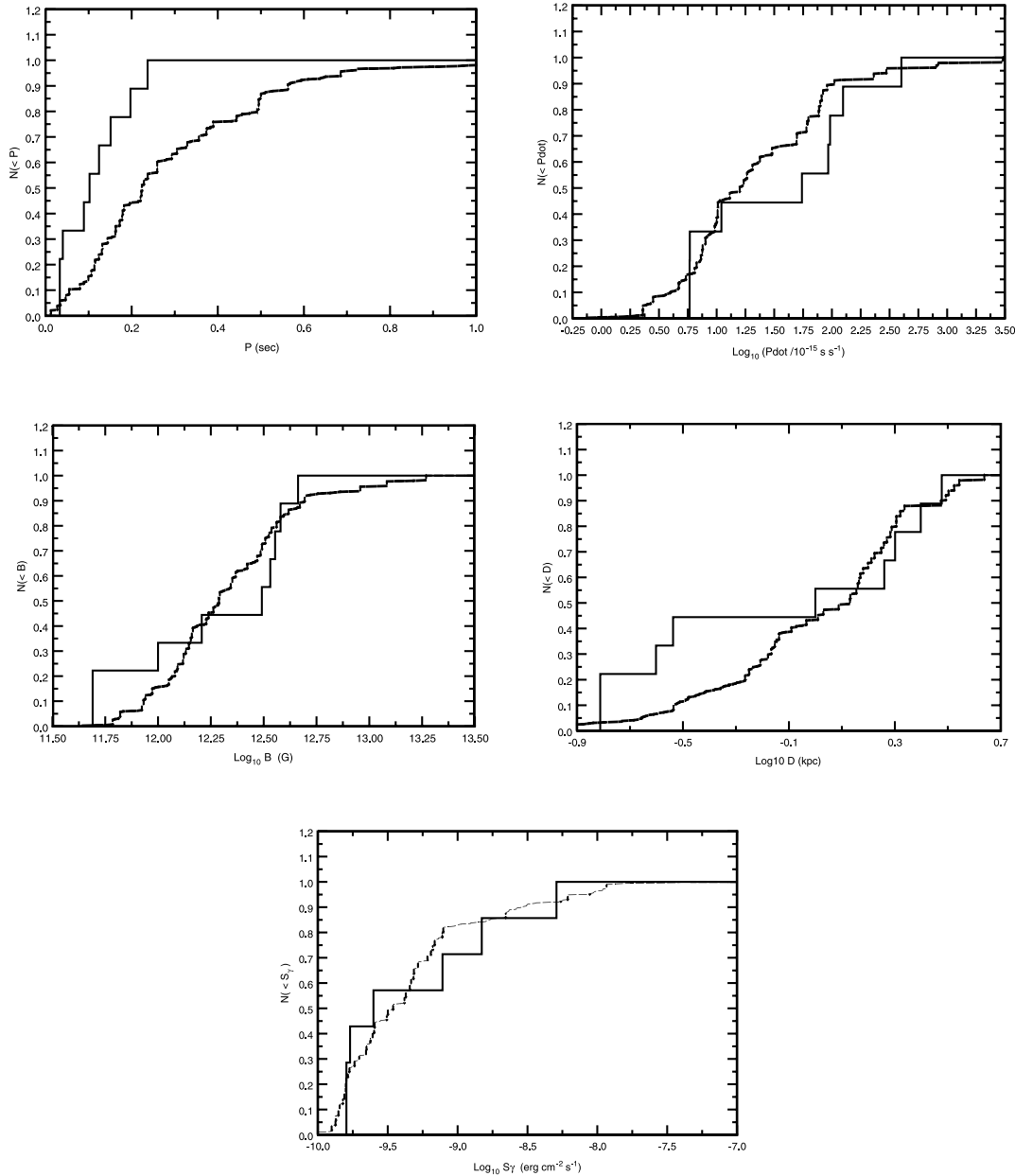


FIG. 5.—Normalized cumulative distributions (*dashed curves*) of period, period derivative, magnetic field, distance, and  $\gamma$ -ray energy flux of  $\gamma$ -ray pulsar population for our model with radio selection effects. For comparison, corresponding distributions (*solid lines*) of the observed  $\gamma$ -ray pulsars are also shown.

We can clearly see that there are two classes of  $\gamma$ -ray pulsars. The  $\gamma$ -ray pulsars located at  $|b| < 5^\circ$  have shorter periods, younger, larger inclination angles, and smaller outer gap size, compared with  $\gamma$ -ray pulsars located at  $|b| > 5^\circ$ . As we have mentioned,  $\gamma$ -ray pulsars in high Galactic latitude are dominated by mature pulsars, which are old enough to move up the high latitude and to evolve to longer periods. Young  $\gamma$ -ray pulsars will be dominated in the Galactic plane, which have stronger  $\gamma$ -ray luminosity, larger inclination angles, shorter periods, and larger magnetic fields. In Figure 6,  $\gamma$ -ray pulsars in high Galactic latitude are actually closer than those in the Galactic plane. This is because they are older and weaker  $\gamma$ -ray pulsars, so they must be nearby; otherwise, they cannot be detected.

In Figure 7, we plot  $L_\gamma$  versus  $L_{sd}$ , where the top panel is  $\gamma$ -ray pulsars located at  $|b| < 5^\circ$  and the bottom panel is  $\gamma$ -ray pulsars located at  $|b| > 5^\circ$ . We can see that there are two dis-

tinctive regions. For  $L_{sd} > 3 \times 10^{34}$  ergs  $s^{-1}$ , the relation between  $L_\gamma$  and  $L_{sd}$  is rather scattered. However, for  $L_{sd} < 3 \times 10^{34}$  ergs  $s^{-1}$ ,  $L_\gamma$  is proportional to  $L_{sd}$ . In particular, for the  $\gamma$ -ray pulsars at high latitude, most pulsars satisfy  $L_\gamma \propto L_{sd}$ , which means  $f \sim 1$ . This is supported by Figure 6*f*, in which the fractional sizes of the outer gap  $f$  for  $\gamma$ -ray pulsars located at  $|b| > 5^\circ$  are all close to unity, whereas the fractional sizes of the outer gap for  $\gamma$ -ray pulsars located at  $|b| < 5^\circ$  have a wide distribution. If  $L_\gamma \propto L_{sd}^\beta$  is used to fit all  $\gamma$ -ray pulsars, then  $\beta \sim 0.3$  for  $\gamma$ -ray pulsars located at  $|b| < 5^\circ$  and  $\beta \sim 0.6$  for  $\gamma$ -ray pulsars located at  $|b| > 5^\circ$ , respectively. Since the outer gap size is a function of  $B$ ,  $P$ , and  $\alpha$ , for young pulsars, there are more combinations of these three parameters to make the outer gap size less than unity. On the other hand, the periods for old  $\gamma$ -ray pulsars are already so long that there is not much room for the other two parameters to

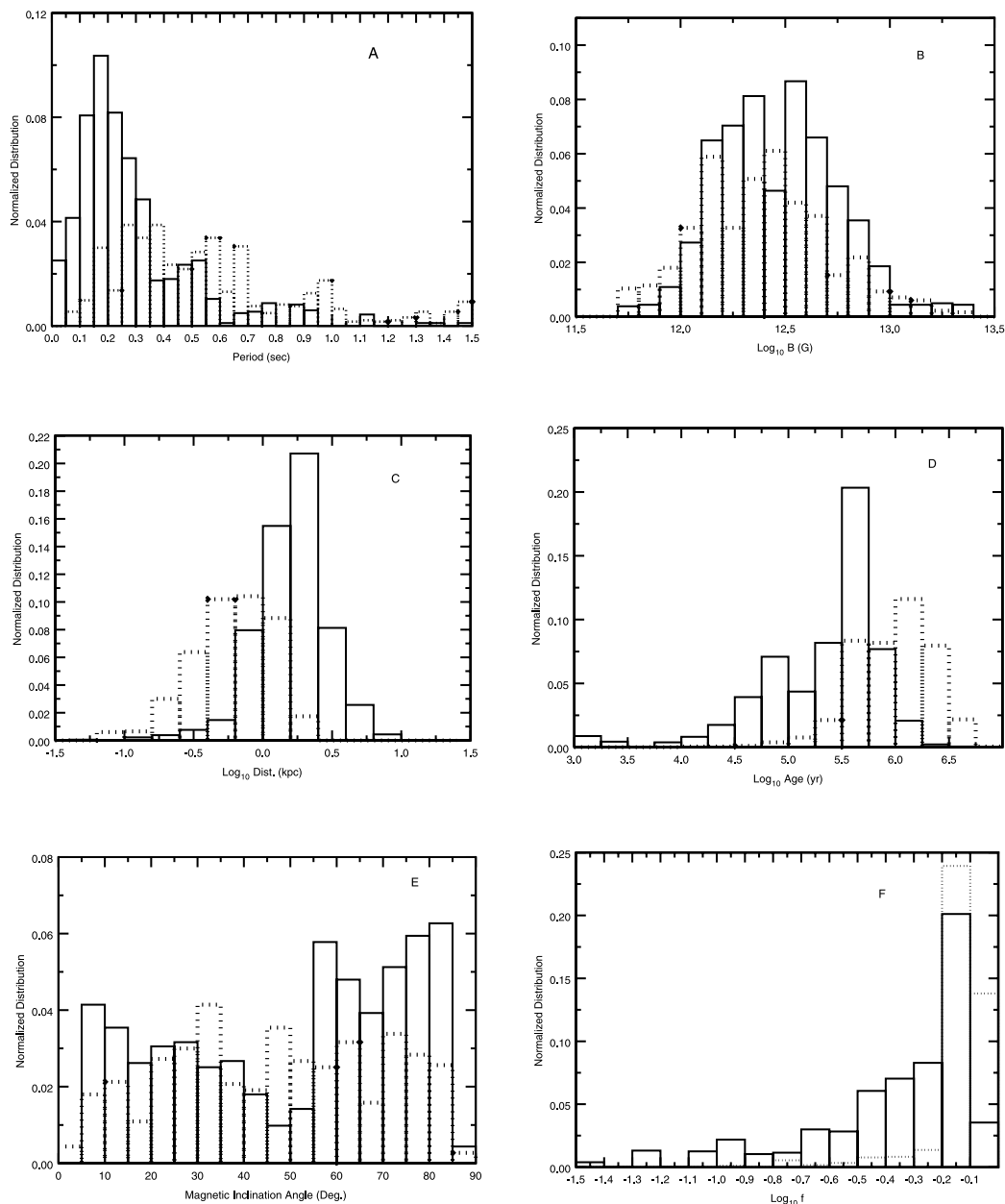


FIG. 6.—Normalized cumulative distributions of period, magnetic field, distance, age, inclination angle, and the average fractional size of outer gap of both simulated  $\gamma$ -ray pulsars in  $|b| \leq 5^\circ$  (solid lines) and  $|b| > 5^\circ$  (dashed lines), which are labeled A, B, C, D, E, and F, respectively.

vary the outer gap size away from unity. The spatial distributions of  $\gamma$ -ray pulsars are given in Figure 8.

In Figures 9a–9d, we compare distributions of  $\gamma$ -ray pulsars from the Galaxy (dotted lines) and from the Gould Belt (solid lines). We can see that the properties of  $\gamma$ -ray pulsars from two sources are very similar, except that  $\gamma$ -ray pulsars from the Gould Belt have lower populations and are closer. These two properties result from the lower birth rate in the Gould Belt, and the solar system is inside the Gould Belt.

## 6. CONCLUSION AND DISCUSSION

We have studied the  $\gamma$ -ray emission properties of pulsars in the Galaxy as well as in the Gould Belt by using a new self-consistent outer gap model, which includes the effects of the inclination angle and average properties of the outer gap. We have found that this new model can produce more mature

$\gamma$ -ray pulsars, which have longer period, smaller inclination angles, and typical ages of 1 million yr old, than the old model. In fact, the mature  $\gamma$ -ray pulsars dominate in high Galactic latitude. The spectra of these mature pulsars are significantly softer and weaker than the young pulsars in the Galactic plane, because the spectral hardness is roughly determined by the typical photon energy given in equation (1), which characterizes the position of spectral break. The explicit proof of the typical photon energy's dependence on the inclination angle is given in equations (28) and (38) of Zhang et al. (2004). Although the form is quite complicated, we can roughly understand why a smaller inclination angle gives smaller typical photon energy and hence a softer spectrum by equation (1). This is because the typical position of the outer gap is the null surface, which becomes larger for smaller inclination angles. From the simulation results, it is not clear why  $\gamma$ -ray pulsars at

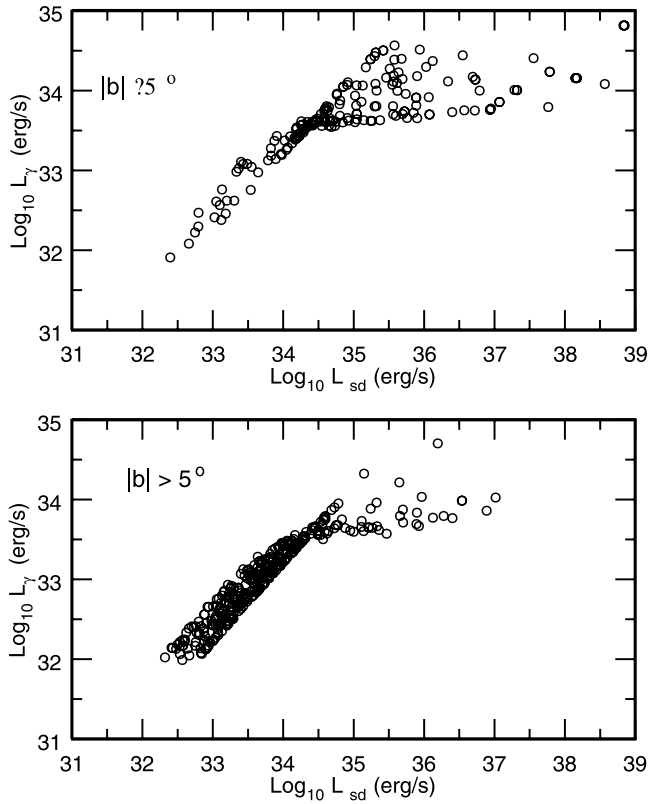


FIG. 7.—Plot of  $\gamma$ -ray luminosity vs. spin-down luminosity for the simulated  $\gamma$ -ray pulsars. Top:  $|b| \leq 5^\circ$ ; bottom:  $|b| > 5^\circ$ .

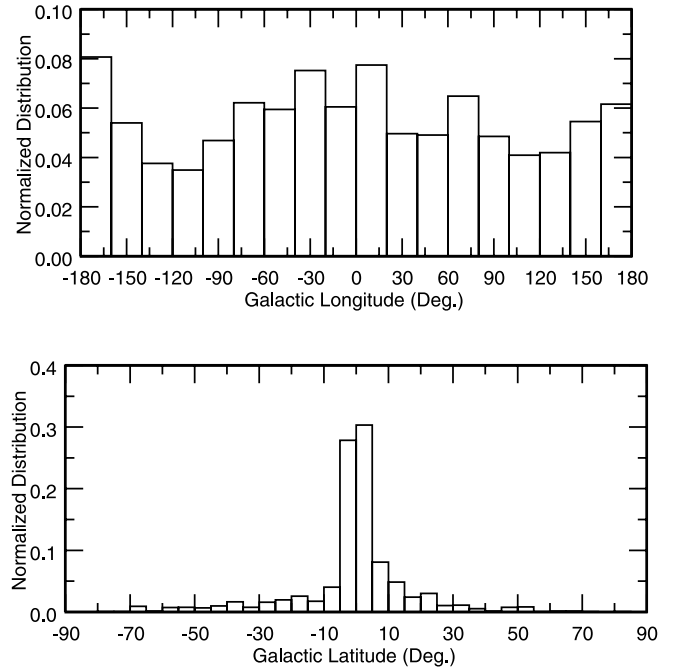


FIG. 8.—Normalized distributions of the simulated  $\gamma$ -ray pulsars in Galactic longitude and latitude.

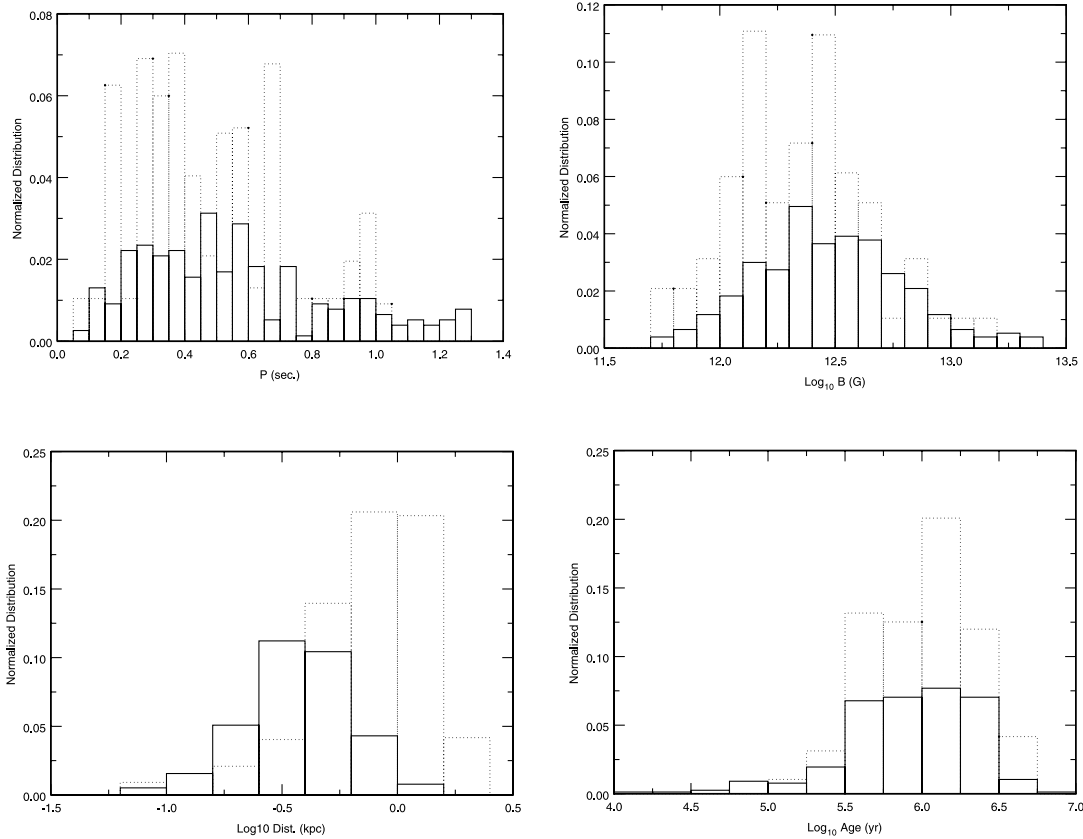


FIG. 9.—Normalized distributions of period, magnetic field, distance, and age of the simulated  $\gamma$ -ray pulsars for  $|b| > 5^\circ$ . Dotted histograms represent the distributions of the simulated  $\gamma$ -ray pulsars without those produced in the Gould belt, and solid histograms represent the simulated  $\gamma$ -ray pulsars only produced in the Gould belt.

high latitude should have smaller inclination angles. This is because all of these high latitude pulsars are older pulsars, which have longer periods. Without the compensation of the effect of inclination angle, the fractional size of the outer gap  $f$  is larger than unity (cf. eq. [3]). In order to maintain the outer gap size at less than unity,  $\eta$  in equation (4), which contains the effect of inclination angle, must be small. In fact,  $\eta$  becomes small for small inclination angles (cf. Fig. 1 of Zhang et al. 2004). Therefore, high-latitude  $\gamma$ -ray pulsars tend to have smaller inclination angles and harder spectra. On the other hand, this seems to imply that the confirmed radio-loud  $\gamma$ -ray pulsars in the Galactic plane should have larger inclinations. This statistical correlation has not yet been established. However, we would like to point out that the values of inclination angles of pulsars are very difficult to measure accurately, and there are only seven confirmed  $\gamma$ -ray pulsars. Thus, it is very difficult to find such correlation in radio-loud  $\gamma$ -ray pulsars. However, we do believe that this correlation should be there when more radio-loud  $\gamma$ -ray pulsars are discovered in the Galactic plane.

We have also used a Monte Carlo method to simulate the properties of the  $\gamma$ -ray pulsar population in the Galaxy as well as in the nearby Gould Belt in terms of the revised outer gap models. The initial magnetic field, spatial, and velocity distributions of the neutron star at birth, which are obtained by the radio pulsar statistical studies, have been used in our simulations. We have obtained the spatial, distance, period, age, magnetic field, inclination angle, and photon flux distributions of the radio-loud and radio-quiet  $\gamma$ -ray pulsars. We find that the properties of  $\gamma$ -ray pulsars between  $|b| < 5^\circ$  and  $|b| > 5^\circ$  are very different. Galactic plane  $\gamma$ -ray pulsars are younger, shorter in period, and have larger inclination angles.

They satisfy different relations between  $L_\gamma$  and  $L_{sd}$ . The high-latitude  $\gamma$ -ray pulsars satisfy  $L_\gamma \propto L_{sd}^{0.6}$ , but the Galactic plane pulsars satisfy  $L_\gamma \propto L_{sd}^{0.3}$ .

The present model predicts very similar numbers of  $\gamma$ -ray pulsars as old models, but many more high latitude  $\gamma$ -ray pulsars than old models (Cheng & Zhang 1998; Zhang et al. 2000). This is because the new model allows the outer gap to exist for about a few million years for appropriate combinations of  $B$ ,  $P$ , and  $\alpha$ , so that old  $\gamma$ -ray pulsars can move up to high Galactic latitude. Furthermore, the nearby Gould Belt also contributes a significant number of  $\gamma$ -ray pulsars at high latitude. Torres & Nuza (2003) have predicted that *AGILE* can detect more  $\gamma$ -ray pulsars (for a general review of *AGILE*, cf. Tavani et al. 2001). Perhaps *AGILE* can provide some clues to differentiate polar gap model predictions (Gonthier et al. 2002) and outer gap model predictions, and *GLAST* makes the final verdict. Finally, we comment that better predictions of how many  $\gamma$ -ray pulsars should be detected by *AGILE* and *GLAST* should include a better expression of the  $\gamma$ -ray solid angle, which depends on the inclination angle as well as the outer gap size. However, in order to have a reliable expression of the  $\gamma$ -ray solid angle, we need to carry out three-dimensional model calculations and come up with an approximate expression from Monte Carlo simulations.

We thank an anonymous referee for the very useful comments. This work is partially supported by an RGC grant from the Hong Kong Government, the ‘‘Hundred Talents Program of CAS,’’ and the National 973 Projection of China (NKBRSGF 19990754).

#### REFERENCES

- Arons, J., & Scharlemann, E. T. 1979, *ApJ*, 231, 854  
 Becker, W., et al. 2003, *ApJ*, 594, 798  
 Bhattacharya, D., Wijers, R. A. M. J., Hartman, J. W., & Verbunt, F. 1992, *A&A*, 254, 198  
 Biggs, J. D. 1990, *MNRAS*, 245, 514  
 Cheng, K. S., Ho, C., & Ruderman, M. A. 1986a, *ApJ*, 300, 500 (CHRI)  
 ———. 1986b, *ApJ*, 300, 522 (CHRII)  
 Cheng, K. S., Ruderman, M., & Zhang, L. 2000, *ApJ*, 537, 964  
 Cheng, K. S., & Zhang, J. L. 1996, *ApJ*, 463, 271  
 ———. 1998, *ApJ*, 498, 327  
 ———. 1999, *ApJ*, 515, 337  
 Daugherty, J. K., & Harding, A. K. 1996, *ApJ*, 458, 278  
 Emmering, R. T., & Chevalier, R. A. 1989, *ApJ*, 345, 931  
 Fan, G. L., Cheng, K. S., & Manchester, R. N. 2001, *ApJ*, 557, 297  
 Fichtel, C. E., et al. 1994, *ApJ*, 434, 557  
 Gehrels, N., et al. 2000, *Nature*, 404, 363  
 Gonthier, P. L., Ouellette, M. S., Berrier, J., O’Brien, S., & Harding, A. K. 2002, *ApJ*, 565, 482  
 Grenier, I. 1997, ‘‘Gamma-Ray Sources and Diffuse Emission Above 100 MeV,’’ talk presented at Workshop on High Energy Cosmic Neutrinos (June 1997, Marseille, France), E6  
 ———. 2000, *A&A*, 364, L93  
 Guillout, P., et al. 1998, *A&A*, 337, 113  
 Haberl, F., et al. 2003, *A&A*, 403, L19  
 Halpern, J. P., Gotthelf, E. V., Mirabal, N., & Camilo, F. 2002, *ApJ*, 573, L41  
 Halpern, J. P., & Ruderman, M. A. 1993, *ApJ*, 415, 286  
 Harding, A. K., & Muslimov, A. G. 1998, *ApJ*, 508, 328  
 Harding, A. K., & Zhang, B. 2001, *ApJ*, 548, L37  
 Hartman, R. C., et al. 1999, *ApJS*, 123, 79  
 Hirofani, K., & Shibata, S. 2001, *ApJ*, 558, 216  
 Kaaret, P., & Cottam, J. 1996, *ApJ*, 462, L35  
 Kramer, M., et al. 2003, *MNRAS*, 342, 1299  
 Lorimer, D. R., Bailes, M., & Harrison, P. A. 1997, *MNRAS*, 289, 592  
 Manchester, R. N., et al. 2001, *MNRAS*, 328, 17  
 McLaughlin, M. A., Mattox, J. R., Cordes, J. M., & Thompson, D. J. 1996, *ApJ*, 473, 763  
 Mirabal, N., & Halpern, J. P. 2001, *ApJ*, 547, L137  
 Mirabal, N., et al. 2000, *ApJ*, 541, 180  
 Montmerle, T. 1979, *ApJ*, 231, 95  
 Moreno, E., Alfaro, E. J., & Franco, J. 1999, *ApJ*, 522, 276  
 Narayan, R., & Ostriker, J. P. 1990, *ApJ*, 352, 222  
 Nolan, P. L., Tompkins, W. F., Grenier, I. A., & Michelson, P. F. 2003, *ApJ*, 597, 615  
 Olano, C. A. 1982, *A&A*, 112, 195  
 Paczynski, B. 1990, *ApJ*, 348, 485  
 Press, W., Flannery, B., Teukolsky, S., & Vetterling, W. 1992, *Numerical Recipes in Fortran: The Art of Scientific Computing* (2nd ed.; Cambridge: Cambridge Univ. Press)  
 Romero, G. E., Benaglia, P., & Torres, D. F. 1999, *A&A*, 348, 868  
 Romero, G. E., Combi, J. A., & Colomb, F. R. 1994, *A&A*, 288, 731  
 Sanwal, D., Pavlov, G., Zavlin, V., & Teter, M. 2002, *ApJ*, 574, L61  
 Sturmer, S. J., & Dermer, C. D. 1996, *ApJ*, 461, 872  
 Tavani, M., et al. 2001, in *AIP Conf. Proc.* 587, *Gamma 2001: Gamma-Ray Astrophysics*, ed. S. Ritz, N. Gehrels, & C. R. Shrader (Melville: AIP), 729  
 Torres, D. F., Butt, Y. M., & Camilo, F. 2001, *ApJ*, 560, L155  
 Torres, D. F., & Nuza, S. E. 2003, *ApJ*, 583, L25  
 Yadigaroglu, I. A., & Romani, R. W. 1995, *ApJ*, 449, 211  
 ———. 1997, *ApJ*, 476, 347  
 Zhang, L., & Cheng, K. S. 1997, *ApJ*, 487, 370  
 ———. 1999, *ApJ*, 526, 327  
 Zhang, L., Cheng, K. S., Jiang, Z. J., & Leung, P. 2004, *ApJ*, 604, 317  
 Zhang, L., Zhang, Y. J., & Cheng, K. S. 2000, *A&A*, 357, 957